Journal of Zhejiang University-SCIENCE B (Biomedicine & Biotechnology) *2025 26(3):254-268*
www.jzus.zju.edu.cn; www.springer.com/journal/11585
E-mail: jzus_b@zju.edu.cn

Research Article

https://doi.org/10.1631/jzus.B2300531

SP7 transcription factor ameliorates bone defect healing in low-density lipoprotein receptor-related protein 5 (LRP5)-dependent osteoporosis mice

Yue XI[1*], Qifeng JIANG[2*], Wei DAI[1], Chaozhen CHEN[1], Yang WANG[1], Xiaoyan MIAO[1], Kaichen LAI[1], Zhiwei JIANG[1], Guoli YANG[1✉], Ying WANG[1✉]

[1]*Stomatology Hospital, School of Stomatology, Zhejiang University School of Medicine, Zhejiang Provincial Clinical Research Center for Oral Diseases, Key Laboratory of Oral Biomedical Research of Zhejiang Province, Cancer Center of Zhejiang University, Engineering Research Center of Oral Biomaterials and Devices of Zhejiang Province, Hangzhou 310000, China*
[2]*School of Stomatology, Zhejiang University, Hangzhou 310058, China*

Abstract: Loss-of-function variants of low-density lipoprotein receptor-related protein 5 (LRP5) can lead to reduced bone formation, culminating in diminished bone mass. Our previous study reported transcription factor osterix (SP7)-binding sites on the *LRP5* promoter and its pivotal role in upregulating LRP5 expression during implant osseointegration. However, the potential role of SP7 in ameliorating LRP5-dependent osteoporosis remained unknown. In this study, we used mice with a conditional knockout (cKO) of *LRP5* in mature osteoblasts, which presented decreased osteogenesis. The in vitro experimental results showed that SP7 could promote LRP5 expression, thereby upregulating the osteogenic markers such as alkaline phosphatase (*ALP*), Runt-related transcription factor 2 (*Runx2*), and *β-catenin* ($P<0.05$). For the in vivo experiment, the SP7 overexpression virus was injected into a bone defect model of *LRP5* cKO mice, resulting in increased bone mineral density (BMD) ($P<0.001$) and volumetric density (bone volume (BV)/total volume (TV)) ($P<0.001$), and decreased trabecular separation (Tb.Sp) ($P<0.05$). These data suggested that SP7 could ameliorate bone defect healing in *LRP5* cKO mice. Our study provides new insights into potential therapeutic opportunities for ameliorating LRP5-dependent osteoporosis.

Key words: Gene therapy; Low-density lipoprotein receptor-related protein 5 (LRP5); Transcription factor osterix (SP7); Osteoporosis; Defect healing

1 Introduction

Osteoporosis, a severe public health problem, is characterized by decreased bone density and reduced bone strength, eventually leading to skeletal dysfunction. Age, sex, hormones, physical activity, nutrition, hereditary factors, and environmental factors have all been reported to contribute to osteoporosis (Castrogiovanni et al., 2016; Cauley and Giangregorio, 2020; Muñoz-Garach et al., 2020; He et al., 2023; Cai et al., 2024). Among these variables, genetic factors play a crucial role in the development of osteoporosis. Wingless/integrated (Wnt)/β-catenin signaling, the canonical branch of Wnt signaling, is a critical regulator in many skeletal physiological and pathological conditions (Baron and Kneissel, 2013; Knight et al., 2018), and has become one of the prime candidates for translational applications during bone regeneration (Leucht et al., 2019; Xu et al., 2022). Low-density lipoprotein receptor-related protein 5 (LRP5) is a coreceptor in the canonical Wnt signaling cascade that regulates bone metabolism (Katchkovsky et al., 2022). Previous studies have revealed the association between *LRP5* mutations and human skeletal disorders, including osteoporosis-pseudoglioma syndrome (OPPG) caused by loss-of-function mutations in *LRP5* (Gong et al., 2001). Additionally, genetic manipulation resulting in

✉ Guoli YANG, guo_li1214@zju.edu.cn
Ying WANG, 7314032@zju.edu.cn
* The two authors contributed equally to this work
Guoli YANG, https://orcid.org/0000-0002-1780-8757
Ying WANG, https://orcid.org/0000-0001-6983-508X
Yue XI, https://orcid.org/0000-0002-8001-8969

Received Aug. 1, 2023; Revision accepted Nov. 30, 2023;
Crosschecked Jan. 2, 2025; Published online Mar. 1, 2025

a gain-of-function of *LRP5* induced a high bone mass phenotype in humans (Hofbauer et al., 2002; Little et al., 2002). The above evidence suggests that *LRP5* is a highly desirable therapeutic target to ameliorate osteoporosis and promote bone regeneration. Our previous studies have also confirmed that *LRP5* might be a potential therapeutic gene for enhancing bone regeneration during implant osseointegration (Jiang et al., 2017, 2020).

In the past several years, the pharmacologic blockade of secreted inhibitors of Wnt signaling has received considerable attention for the purpose of LRP5-dependent osteoporosis therapy (Witcher et al., 2018). Nevertheless, the possibility of gene therapy to directly activate *LRP5* warrants further investigation. Transcription factors directly interpret the genome and function as "master regulators" and "selector genes" to perform the first step in decoding the DNA sequence (Lambert et al., 2018). Transcription factor-based therapies have demonstrated great potential in achieving tissue regeneration, including bone, cartilage, and cardiac regeneration (Song KH et al., 2012; Lee and Young, 2013; Rilo-Alvarez et al., 2021). The zinc finger protein SP7 is an indispensable transcription factor that activates an array of genes involved in osteoblast differentiation within developing and mature bones (Fukuda et al., 2018). A previous study claimed that SP7 null mice lacked mature osteoblasts (Nakashima et al., 2002). Despite its significance in physiological homeostasis, the specific molecular functions of SP7 have yet to be fully elucidated (Hoshikawa et al., 2020; Wang et al., 2021). Similar to other SP family members, SP7 is initially posited to bind to GC-rich promoter/enhancer sequences to activate the osteogenic transcriptional network in osteoblasts (Hafner et al., 1995). However, evidence has emerged that the preference of SP7 for AT-rich promoter/enhancer sequences, distinct among SP proteins, is critical for osteoblast differentiation (Lui et al., 2022). Another recent study demonstrated that SP7 likely interacts with different enhancer DNA motifs at different osteoblast lineage stages to regulate enhancer activity (Wang et al., 2021). Given its unique role in osteoblast differentiation, *SP7* might be a promising therapeutic gene for tissue regeneration.

Wnt signaling, enhanced by activating mutations in *LRP5*, leads to the upregulation of SP7 expression (Lim et al., 2015). Conversely, SP7 expression is diminished in osteoblast precursor-specific β-catenin conditional knockout (cKO) mice and osteoblast-specific Wntless cKO mice (Hill et al., 2005; Zhong et al., 2012). Our recent study reported two SP7-binding sites on the rat *LRP5* promoter, indicating a direct regulatory relationship between SP7 and *LRP5*. The important role of the SP7/LRP5 axis during early implant osseointegration has also been confirmed (Yu et al., 2022). Of note, it remains unknown whether SP7 regulates LRP5 expression to trigger a cascade of downstream signaling events to ameliorate LRP5-dependent osteoporosis in vivo. Thus, we hypothesized that SP7 could positively regulate LRP5 expression to restore osteogenesis in LRP5-dependent osteoporosis mice.

This study aimed to verify whether SP7 could regulate LRP5 expression in vitro and to investigate the potential role of SP7 in ameliorating bone defect healing in LRP5-dependent osteoporosis. Our findings provide novel insights into SP7 as a therapeutic target for osteoporosis treatment.

2 Materials and methods

2.1 Mouse model generation and maintenance

LRP5$^{fl/fl}$ mice, B6N.FVB-Tg(BGLAP-Cre)1Clem/J (Oc-Cre) transgenic mice were purchased from The Jackson Laboratory (USA). B6/JGpt-Rosa26$^{tm1(CAG\text{-}LSL\text{-}Cas9\text{-}tdTomato)/Gpt}$ (TdT) transgenic mice were obtained from Gem Pharmatech (Nanjing, China). To determine the genotype of transgenic mice, polymerase chain reaction (PCR) analyses were conducted on genomic DNA extracted from mouse tails. The primers utilized for genotyping the floxed *LRP5* knockout allele are listed in Table S1. The mice were provided with a standard diet and housed under controlled climate with unrestricted access to food. All animal care and experimental procedures were approved by the Animal Research Committee of Zhejiang University (Hangzhou, China) and conducted following international standards. The animals were administered an intraperitoneal injection of alizarin (red) (30 μg/g; ScienCell, USA) at 10 d and calcein (green) (10 μg/g; Sigma-Aldrich, USA) at 3 d before being sacrificed. At 4, 8, 12, and 16 weeks, the male and female transgenic mice were harvested.

2.2 Whole-mount skeletal staining

Skeletal staining allows the measurement of shapes and sizes of individual skeletal elements in their proper

positions; therefore, it is a principal method for detecting skeletal changes. In addition, different types of staining make it feasible to distinguish cartilage from bone, facilitating the determination of skeletal maturity rate (Rigueur and Lyons, 2014; Mead, 2020). To prepare the embryos for this process, they were subjected to brief scalding in hot tap water at 65 ℃ for 1 min, after which the skin and viscera were removed. The embryos were then fixed in 95% (volume fraction) ethanol for 1–2 d, followed by soaking in acetone for 2 d. Lastly, the embryos were submerged in Alcian blue (300 mg Alcian Blue 8 GX in a mixture of 80 mL of 100% ethanol and 20 mL of glacial acetic acid) for cartilage staining for 1–2 d. They were then destained twice in 70% ethanol and incubated in 95% ethanol overnight. The 95% ethanol was subsequently removed and 2% (20 g/L) KOH solution was added for 12–24 h at room temperature until nearly all soft tissues disappeared. The next step involved the replacement of the 2% KOH solution with a solution of alizarin red S (5 mg of alizarin red S in 100 mL of 1% (10 g/L) KOH), in which the embryos were soaked for 12 h at room temperature. Subsequently, the embryos underwent a series of clearing processes, including immersion in 1% KOH, followed by a mixture of 50% KOH (1%) and 50% glycerol, and then a mixture of 50% ethanol and 50% glycerol. The embryos were finally transferred to 100% glycerol for preservation.

2.3 Isolation and culture of cells

Six- to eight-week-old wild-type (WT) mice were used to isolate the bone marrow mesenchymal stem cells (BMSCs). Briefly, the mice were sacrificed by decapitation under deep anesthesia with 3% (30 g/L) pentobarbital sodium. To prepare the mice for analysis, their entire body was immersed in 75% ethanol for 1 min. The tibias and femurs were then separated and a 2.5-mL syringe was used to aspirate the BMSCs from the bone marrows. Osteoblasts were isolated from the tibias and femurs of 3-week-old male WT and cKO mice by enzymatic digestion in α-minimum essential medium (α-MEM) (Biological Industries, Israel) with 0.1% (1 g/L) collagenase (Sigma-Aldrich). BMSCs and osteoblasts were both cultured in basal medium comprising α-MEM containing 10% (volume fraction) fetal bovine serum (FBS; Gibco, USA), 0.272 g/L L-glutamine (Sigma-Aldrich), 1% (0.01 g/mL) penicillin (Gibco), and 1% (0.01 g/mL) streptomycin (Gibco).

2.4 Immunofluorescence microscopy

A total of 1×10^5 osteoblasts per well, derived from both WT and cKO mice, were seeded in 12-well plates and subjected to immunofluorescence assay. Following fixation with 4% (0.04 g/mL) paraformaldehyde, the nuclei of the samples were stained with 4',6-diamidino-2-phenylindole (DAPI; Solarbio, China) for 10–15 min. Subsequently, images were captured using a Zeiss Axio Observer A1 microscope (Germany).

2.5 Flow cytometry

Passage 2 BMSCs with a density of 2×10^6 cells/mL were suspended in ice-cold phosphate-buffered saline (PBS) and incubated with the following antibodies: phycoerythrin (PE) anti-mouse/rat cluster of differentiation 29 (CD29) antibody (102208; Biolegend, San Diego, USA), PE anti-mouse/human CD44 antibody (103008; Biolegend), PerCP/Cyanine5.5 anti-mouse/human CD11b antibody (101228; Biolegend), and PE anti-mouse CD45 antibody (147712; Biolegend). Flow cytometry (FCM) analysis was performed in a CytoFLEX LX multicolor analyzer (Beckman Coulter, Brea, CA, USA), and data analysis was conducted using FlowJo V10 (FlowJo, LLC, Ashland, USA).

2.6 Construction and transfection of *LRP5* and *SP7*

In order to evaluate the potential regulatory effect of SP7 on LRP5, lentiviral vector interfering *LRP5*, interfering lentiviral vector negative control (LV5-NC), lentiviral vector overexpressing *SP7*, and overexpressing lentiviral vector negative control (LV3-NC) were prepared by GenePharma (Shanghai, China). BMSCs were characterized before experimentation. The FCM analysis of passage 2 BMSCs showed that BMSCs were positive for the stemness markers CD29 (99.98%) and CD44 (99.00%) but showed no expression of the negative marker CD11b (0.06%) or CD45 (0.22%) (Fig. S1). Then, BMSCs were seeded at a density of 3×10^5 cells/well in six-well dishes and divided into four groups according to the order of transfection with the lentivirus constructs: (1) control group, transfected with LV5-NC first and then with LV3-NC; (2) $SP7^+$ group, transfected with LV5-NC first and then with lentiviral vector overexpressing SP7; (3) $LRP5^-$ group, transfected with lentiviral vector interfering LRP5 first and then with LV3-NC; (4) $LRP5^-/SP7^+$ group, transfected with lentiviral vector interfering LRP5 first and then with lentiviral vector overexpressing SP7.

2.7 Alkaline phosphatase and alizarin red S staining

The early osteogenic ability of BMSCs after transfection with the corresponding lentiviral vectors was evaluated through alkaline phosphatase (ALP) staining while utilizing the bromochloroindoyl phosphate (BCIP)/nitro blue tetrazolium (NBT) ALP color development kit (C3206, Beyotime, Shanghai, China). The cells were fixed with 4% paraformaldehyde for 15 min, followed by complete coverage with the working solution for 30 min at room temperature. The working solution was subsequently discarded and the cells were rinsed three times with distilled water. The recorded results were subjected to analysis. Next, alizarin red staining was performed to visualize the Ca nodules. After being cultured in osteogenic culture medium (Cyagen Biosciences, Guangzhou, China) for 21 d, cells were fixed in 4% paraformaldehyde for 15 min and then stained with alizarin red (ScienCell, Carlsbad, USA) for 1 h. The results were recorded by a scanner (LaserJet Pro, HP, USA).

2.8 Quantitative PCR

The total RNA of cultured cells was extracted using the TRIzol reagent (Invitrogen, Carlsbad, USA) following culture in osteogenic culture medium, and complementary DNA (cDNA) was synthesized using the PrimeScript™ RT Reagent Kit (Perfect Real Time, TaKaRa, Dalian, China). The concentration of RNA was determined using the NanoDrop 2000 system (Thermo Fisher Scientific, USA). Quantitative real-time PCR (qPCR) was performed using an SYBR Green kit (TaKaRa, Japan) in an ABI ViiATM7 system (Applied Biosystems, Foster City, USA). The relative gene expression of genes was normalized to glyceraldehyde 3-phosphate dehydrogenase (GAPDH) using the $2^{-\Delta\Delta C_T}$ method. The utilized primer sequences are listed in Table S2.

2.9 Western blot analysis

The cells were cultured in osteogenic induction medium for 7 d and then lysed in a combination of radio-immunoprecipitation assay (RIPA) buffer (Beyotime) and 0.1% (volume fraction) protease inhibitor cocktail (Beyotime) for western blot analysis. Tris-glycine sodium dodecyl sulfate-polyacrylamide gel electrophoresis (SDS-PAGE) was employed to separate proteins of equal amounts using a bicinchoninic acid (BCA) kit (Beyotime). Subsequently, the samples were transferred onto polyvinylidene fluoride (PVDF) membranes (Millipore, USA). The membranes were blocked using a blocking buffer consisting of 50 mmol/L Tris-buffered saline (pH 7.4) with 5% (0.05 g/mL) skimmed milk and 0.1% (volume ratio) Tween-20 (TBST). After sectioning into small slices marked with indicators, various membranes were subjected to incubation with distinct primary antibodies at a temperature of 4 °C overnight. Subsequently, the membranes were washed four times for 10 min each with TBST and then exposed to horseradish peroxidase (HRP)-conjugated goat anti-rabbit immunoglobulin G (IgG) (Goodbio Technology, China) for 1 h. Afterwards, the membrane was washed four times for 10 min each with TBST and ultimately exposed using electrochemiluminescence (ECL) solution (Applygen Technologies Inc., China) in a chemiluminescent detection system (Amersham Biosciences, UK). The intensities of the blots were quantified using ImageJ software and normalized to those of GAPDH. The following primary antibodies were used: LRP5 (D80F2; Cell Signaling Technology, USA), SP7 (ab209484; Abcam, USA), β-catenin (ab32752; Abcam), Runt-related transcription factor 2 (Runx2) (ab92336; Abcam), and GAPDH (ab70699; Abcam).

2.10 Surgery

Twelve-week-old male WT and cKO mice were divided into three groups as follows: (1) control group: mice without the injection of SP7 lentiviral vector; (2) LVNC group: mice injected with 1 μL of LVNC into the prepared holes in the tibias; (3) $SP7^+$ group: mice injected with 1 μL of the lentiviral vector overexpressing SP7 into the prepared holes in the tibias. In brief, all the included mice were anesthetized, and then bone defects were created on both sides of the anterior-proximal surfaces of the tibias using 1.2-mm dental stainless steel round drills by sequential drilling under cooled sterile saline irrigation. Subsequently, the muscles were meticulously sutured, with the LVNC and $SP7^+$ groups having undergone lentivirus injection before muscle suturing. Alizarin (red) was intraperitoneally injected into individuals of each group at 10 d, followed by calcein (green) at 3 d before the animals were sacrificed. After a postoperative duration of four weeks, all animals from all groups were collected for analysis.

2.11 Micro-computed tomography

Fully fixed samples were used for the micro-computed tomography (micro-CT) (Scanco Medical, Switzerland) scans. First, the sample was assembled

in a cylindrical sample holder (diameter, 20.5 mm) with the long axis of the sample perpendicular to the X-ray source. The scanning parameters were set to 55 kV and 70 mA. We defined the regions of interest as the areas 0.5 mm proximally away from the growth plate to the distal 100 slices (10 μm per slice). Finally, the microarchitectural parameters were measured directly using the micro-CT Evaluation Program V4.4A (Scanco Medical).

2.12 Specimen preparation and histomorphometric analysis

The dissected samples were fixed in 4% paraformaldehyde for 2 d, and then embedded in 0.5 mol/L ethylenediaminetetraacetic acid (EDTA) disodium solution for three weeks at room temperature for demineralization. Next, hematoxylin-eosin (HE), Masson, tartrate-resistant acid phosphatase (TRAP), Oil red, immunohistochemistry (IHC), and immunofluorescence staining were performed according to standard procedures, and images of HE, Masson, TRAP, Oil red, and IHC were captured under a microscope (Leica, Germany). The immunofluorescence staining images were captured using a confocal laser scanning microscope (Nikon A1, Japan). The TRAP, Oil red, and IHC scores were calculated using ImageJ 1.53a.

2.13 Three-point bending test

In order to assess the biomechanical properties of femurs obtained from twelve-week-old male WT and cKO mice, a small animal bone strength test instrument (YLS-16A; Jinan Yanyi Technology Co., Ltd., Jinan, China) was utilized to conduct a three-point bending experiment. The freshly dissected femurs were promptly subjected to this test using two end support points and one central loading point. Biomechanical measurements were obtained from the load-deformation curves, with the maximum load (N) being recorded.

2.14 Hard tissue sectioning

The samples were dehydrated in a graded ethanol series (70%–100%) and embedded in methyl methacrylate after micro-CT scanning. Slices of the samples were made using a high-speed precision microtome (Leica 2500E, Germany) and ground to a final thickness of 40 mm. Next, the images of samples were observed and captured under a light microscope (Leica).

2.15 Statistics

Statistical analysis was conducted using unpaired, two-tailed Student's *t*-test for comparisons between groups using Prism (GraphPad). The level of statistical significance was set at a P value of <0.05.

3 Results

3.1 Generation of the LRP5-related osteoporosis mouse model and identification of the Oc-Cre-mediated recombination

In order to explore the potential SP7 therapy strategy for LRP5-dependent osteoporosis, an LRP5-related osteoporosis mouse model was generated by crossing a floxed LRP5 ($LRP5^{fl/fl}$) mouse strain with a transgenic mouse that expresses Cre recombinase under the control of the osteocalcin promoter (Oc-Cre) for specific recombination in osteoblasts. To demonstrate the specificity and efficiency of Oc-Cre-mediated recombination, we crossed the established Oc-Cre with TdT to generate the Oc-Cre×TdT reporter mouse model (Fig. 1a). The genotypes were identified by DNA horizontal electrophoresis (Fig. 1b). When constitutively activated, TdT-marked osteolineages express Oc-Cre, which includes bone surface osteoblasts, osteocytes, and osteoprogenitor cell features. Alternatively, by delaying Oc-Cre expression until postnatally, TdT targeting can be restricted to committed osteoblasts and osteocytes. The histological analysis of frozen sections from femurs and mandibles confirmed the presence of TdT^{+} cells (Fig. 1c). Next, to verify the specificity and efficiency of Cre-mediated recombination, osteoblasts were isolated from $LRP5^{fl/fl}$;TdT (WT) and Oc-Cre;$LRP5^{fl/fl}$;TdT (cKO) mice. The fluorescence imaging of osteoblasts from WT and cKO male mice (Fig. 1d) and the FCM analysis of osteoblasts from cKO male mice (Fig. 1e) confirmed the specificity and efficiency of Cre-mediated recombination.

The immunohistochemical results showed that LRP5 was hardly expressed in the femur tissues of cKO mice and its downstream molecule β-catenin was also reduced compared with that in WT mice (Fig. 1f). In addition, qPCR revealed that the messenger RNA (mRNA) expression level of *LRP5* was significantly decreased in osteoblasts from cKO mice compared with that from WT mice (Fig. 1g). Western

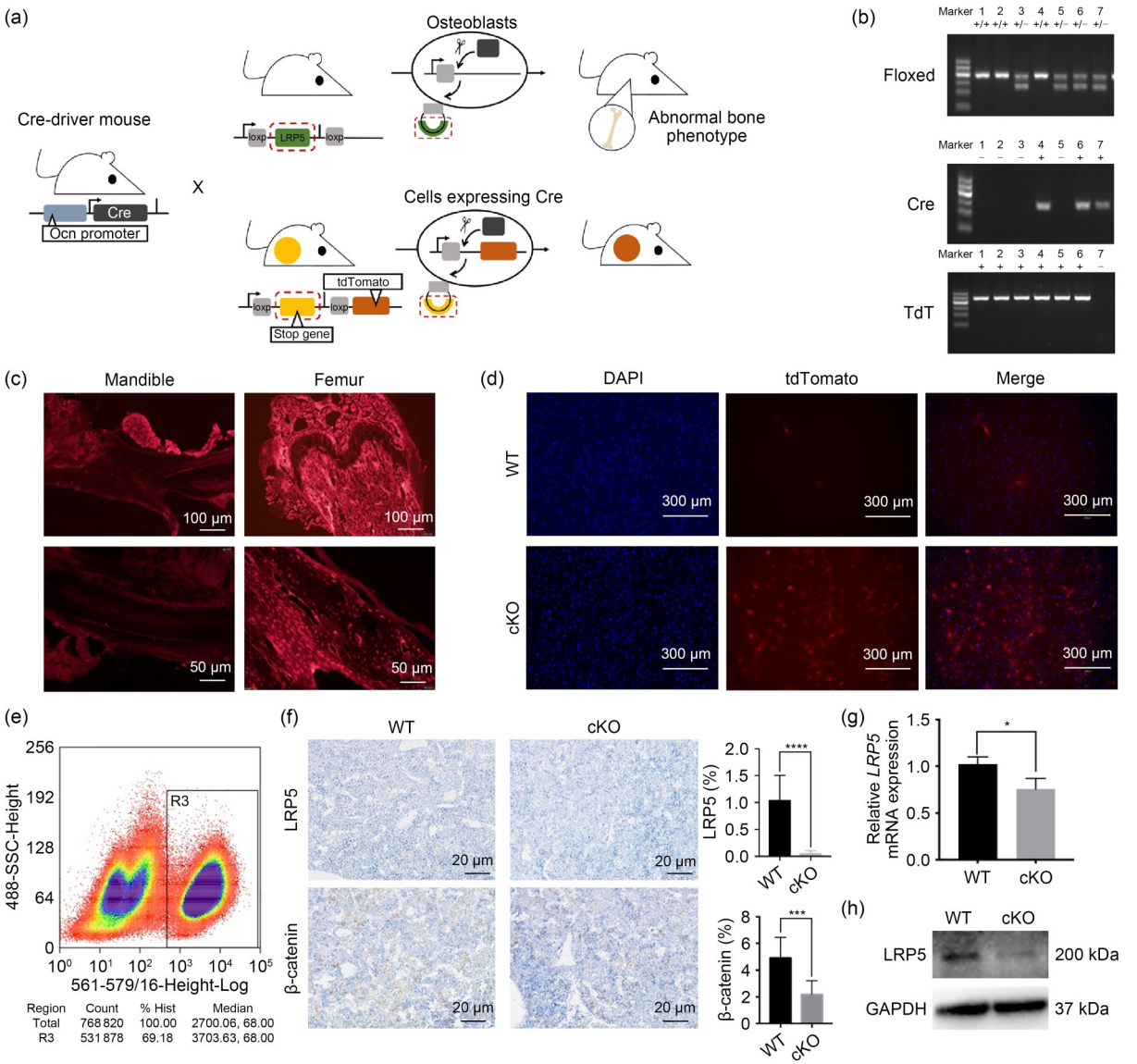

Fig. 1 Specificity and efficiency of Oc-Cre-mediated recombination. (a) The Cre×Cre-reporter breeding strategy used in this study. (b) The genotypes were identified by DNA horizontal electrophoresis identification. (c) Histological analysis of frozen sections from femurs and mandibles of conditional knockout (cKO) mice. (d) Dual fluorescence imaging of osteoblasts from wild-type (WT) and cKO male mice. (e) Flow cytometry (FCM) analysis of osteoblasts from cKO male mice. (f) Immunohistochemical staining and quantification of low-density lipoprotein receptor-related protein 5 (LRP5) and β-catenin from femoral sections of WT and cKO male mice. (g) According to quantitative real-time polymerase chain reaction (qPCR) analysis, the relative messenger RNA (mRNA) expression of *LRP5* was decreased in osteoblasts from cKO mice compared to that from WT mice. (h) Western blot analysis showed decreased protein expression of LRP5 in osteoblasts from cKO mice compared to that from WT mice. Data are expressed as mean±standard deviation (SD) (n=6). * P<0.05, *** P<0.001, **** P<0.0001. Oc-Cre: osteocalcin-Cre; Ocn: osteocalcin; loxp: locus of crossover in P1; tdTomato: tandem dimer tomato; DAPI: 4',6-diamidino-2-phenylindole; GAPDH: glyceraldehyde 3-phosphate dehydrogenase; SCC: side scatter.

blot analysis showed that the protein expression of LRP5 was decreased in osteoblasts from cKO mice compared to that from WT mice (Fig. 1h). These results further proved the successful knockout of *LRP5* in the osteolineages.

3.2 Characterization of morphological phenotypic changes in Oc-Cre;LRP5$^{f/f}$ mice

As a first attempt to evaluate the skeletal development of the two genotypes of mice, we measured

the weight and length of female and male specimens at four weeks of age (Figs. 2a and 2b). The body length of cKO mice was slightly decreased compared with that of WT mice, but the difference was not statistically significant. Furthermore, the two genotypes showed no significant difference in body weight. Newborn mice did not present any obvious systemic developmental defects, which were difficult to distinguish by the naked eye in littermate WT mice (Fig. 2a). We used Alcian blue and alizarin red S whole skeleton staining to examine the development of craniofacial and axial skeletons in cKO mice; cKO neonatal mice had shorter long bones and smaller skulls and mandibles (Fig. 2c). Furthermore, cKO exhibited the phenotype of wide sutures, unclosed fontanelles, and wide cranial sutures. These data revealed that both intramembranous ossification and endochondral ossification were inhibited in cKO mice.

3.3 Effect of Oc-Cre-mediated deletion of LRP5 on bone mass

The histomorphometry of femoral metaphysis was performed to observe osteogenesis and adipogenesis in mice (Fig. 3a). The number and area of trabeculae in the bone marrow cavity of cKO mice were significantly reduced, as shown by HE and Masson staining. As a marker of bone resorptive activity, TRAP expression was elevated in cKO mice. Additionally, the proportion of fat in the medullary cavity was increased in these mice (Figs. 3a and 3b). The fluorochrome labeling of bone 10 and 3 d before sacrifice revealed a progressive pattern of bone formation and mineralization (Fig. 3d). Further morphometric analysis of the femoral bone by micro-CT detected a significant decrease in the trabecular number (Tb.N) in cKO mice compared with that in WT littermates (Figs. 4a and 4b). The

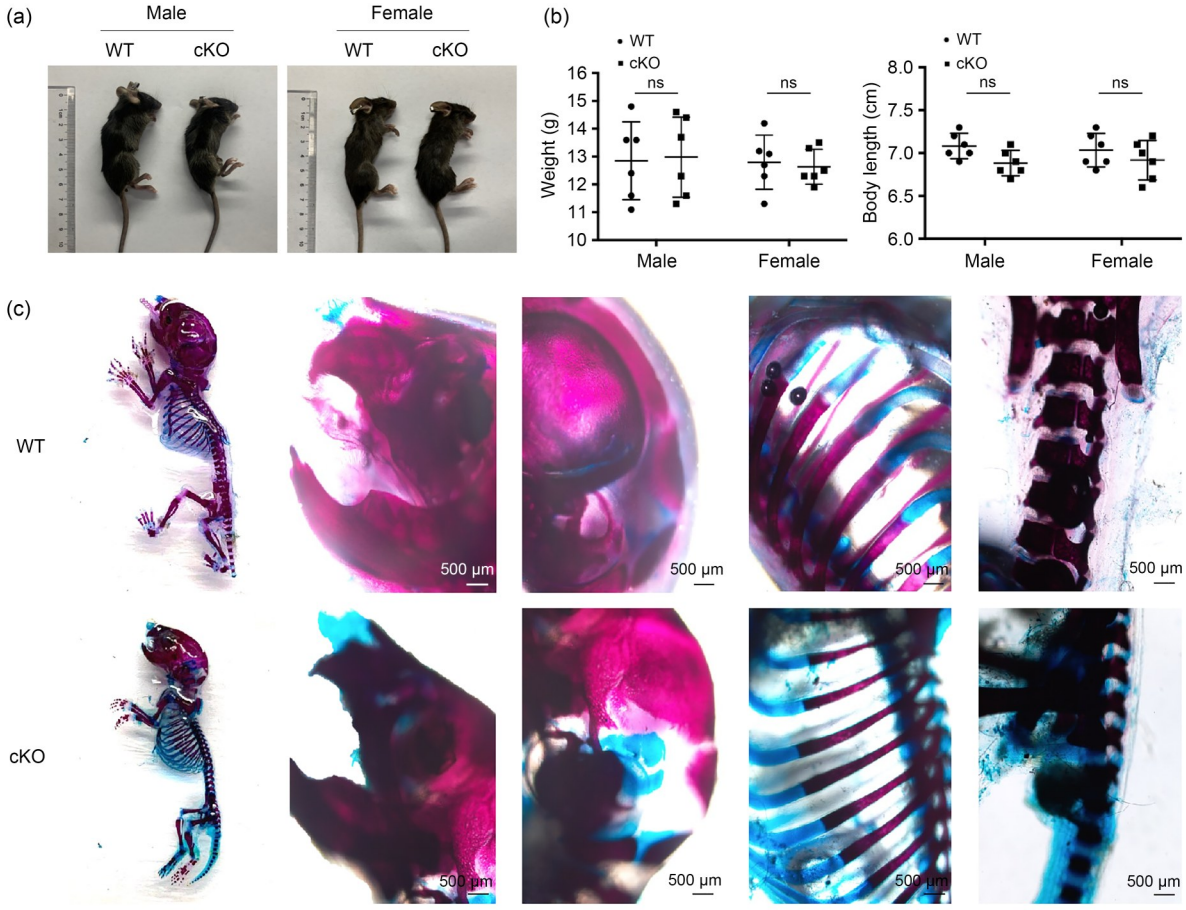

Fig. 2 Characterization of morphological phenotypic changes in Oc-Cre and LRP5$^{f/f}$ mice. (a, b) Weight and length measurements of wild-type (WT) and conditional knockout (cKO) 4-week-old female/male mice. Data are expressed as mean±standard deviation (SD) (weight, *n*=6; body length, *n*=3). (c) Whole-mount skeletal staining of WT and cKO newborn mice. LRP5: low-density lipoprotein receptor-related protein 5; Oc-Cre: osteocalcin-Cre; ns: not significant.

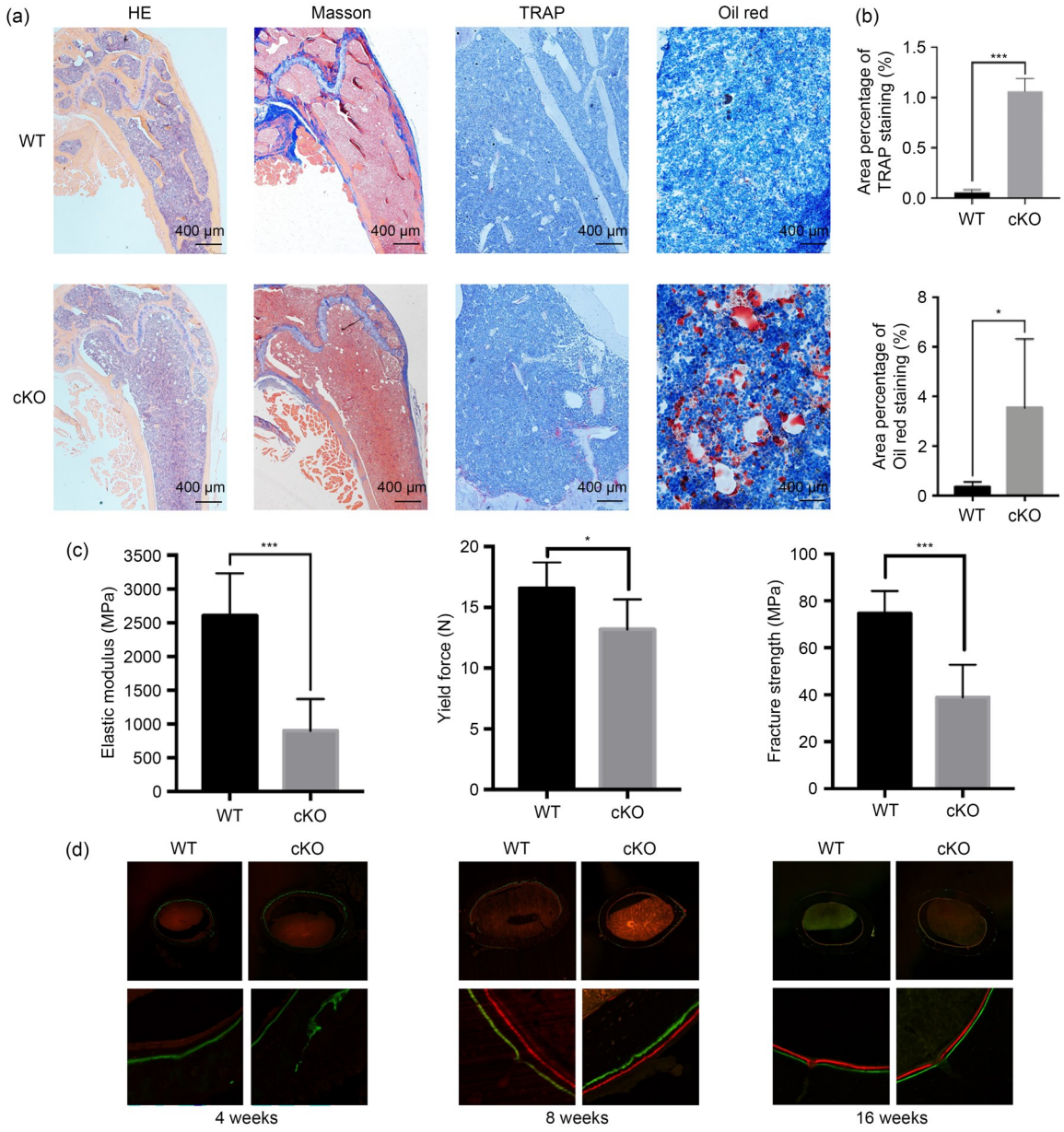

Fig. 3 Effects of LRP5 deletion in Ocn$^+$ osteoblasts on bone impairment and marrow adiposity. (a) Hematoxylin-eosin (HE), Masson, tartrate-resistant acid phosphatase (TRAP), Oil red staining of femoral sections from wild-type (WT) and conditional knockout (cKO) male mice. (b) Area percentage of TRAP and Oil red staining in the distal marrow per tissue area. (c) Three-point bending experiment to evaluate the biomechanical properties of femurs from WT and cKO male mice. The elastic modulus, bone yield strength and fracture strength of cKO mouse femurs were significantly reduced. (d) The images of fluorochrome labeling in the bone marrow of tibial defects from 4-, 8-, and 16-week-old WT and cKO male mice. Data are expressed as mean±standard deviation (SD) (n=6). * P<0.05, *** P<0.001. LRP5: low-density lipoprotein receptor-related protein 5; Ocn$^+$: expressing osteocalcin.

volumetric density (bone volume (BV)/total volume (TV)), bone mineral density (BMD), and Tb.N were significantly reduced in the proximal tibiae of 4-, 8-, and 12-week-old cKO mice compared with those in age- and sex-matched WT mice, while trabecular separation (Tb.Sp) was markedly increased (Fig. 4b).

Using the above detection methods, we could confirm that the BMD and bone mass of cKO mice were significantly lower than those of WT mice. The biomechanical properties of mouse femurs in different groups were analyzed using the three-point bending test (Fig. 3c). Compared with that in WT mice, the

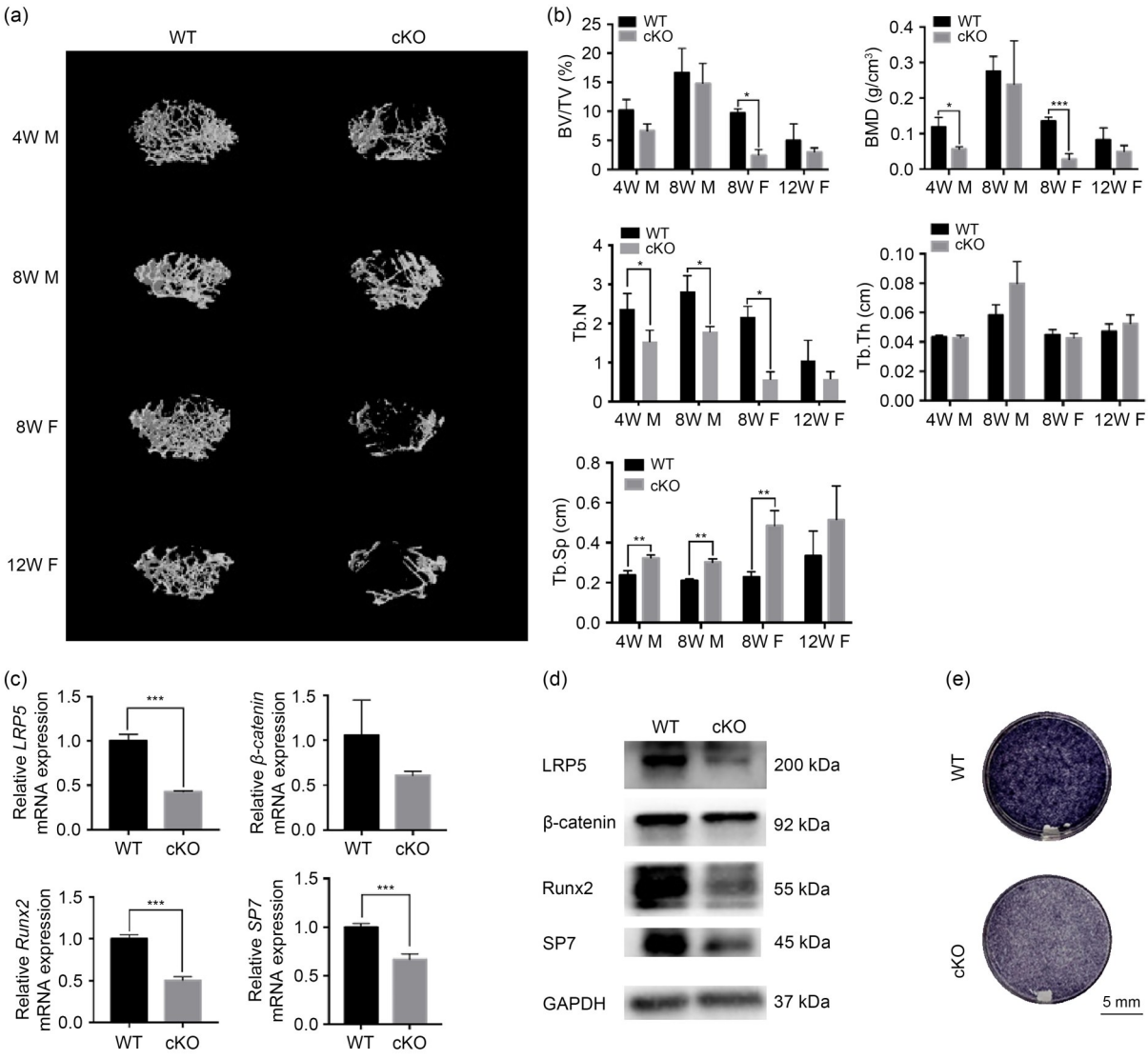

Fig. 4 Relative expression of LRP5 in osteoblasts and expression changes of canonical Wnt signaling target genes. (a) Representative images of micro-computed tomography (micro-CT) reconstruction of trabecular bone structure in the distal femoral head. (b) Quantitative micro-CT analyses of metaphysis region of distal femurs. (c) According to quantitative real-time polymerase chain reaction (qPCR) analysis, the relative messenger RNA (mRNA) expression levels of *LRP5*, *β-catenin*, Runt-related transcription factor 2 (*Runx2*), and transcription factor osterix (*SP7*) were decreased in osteoblasts from conditional knockout (cKO) mice compared to those from wild-type (WT) mice. (d) Western blot analysis showed the protein expression of LRP5, β-catenin, Runx2, and SP7. (e) The alkaline phosphatase (ALP) staining was performed to evaluate the osteogenic ability of osteoblasts from cKO mice compared to those from WT mice on osteogenic Day 7. Data are expressed as mean±standard deviation (SD) (n=6). * P<0.05, ** P<0.01, *** P<0.001. LRP5: low-density lipoprotein receptor-related protein 5; Wnt: wingless/integrated; M: male; F: female; W: weeks; BV/TV: bone volume to tissue volume; BMD: bone mineral density; Tb.N: trabecular number; Tb.Th: trabecular thickness; Tb.Sp: trabecular separation; GAPDH: glyceraldehyde 3-phosphate dehydrogenase.

elastic modulus of cKO mouse femurs was reduced, lowering the bending ability of the femurs in this mouse type. The bone yield and fracture strength were also diminished, with statistical significance. Therefore, the lack of LRP5 in bone tissue was considered to potentially cause bone loss and reduce bone fragility.

qPCR indicated that the mRNA expression levels of *LRP5* and downstream genes, including *β-catenin*, *Runx2*, and *SP7*, were significantly decreased in osteoblasts from cKO mice compared with those from WT mice (Fig. 4c). Western blot analysis showed decreased protein expression levels of LRP5, β-catenin, Runx2,

and SP7 in osteoblasts from cKO mice compared with those from WT mice (Fig. 4d), which suggested that LRP5 played a vital role in bone homeostasis via an LRP5/β-catenin/Runx2/SP7 regulatory loop. Correspondingly, ALP activity was decreased in osteoblasts from WT mice (Fig. 4e).

3.4 Role and mechanism of the SP7/LRP5 signaling axis in the osteogenesis of osteoblasts

Our recent study reported a direct regulatory relationship between SP7 and LRP5 (Wang et al., 2021). To study the role of SP7/LRP5 signaling axis in the osteogenesis of osteoblasts, we constructed cell models in vitro using lentiviral vectors to inhibit or overexpress related genes. ALP activity, detected by ALP staining and semiquantitative methods (Figs. 5a and 5b), was increased in the $SP7^+$ group and decreased in the $LRP5^-$ group. When co-transfected with $LRP5^-$ and $SP7^+$ viruses, the ALP activity was significantly increased compared with that in the $LRP5^-$ group. Similarly, mineralized nodules were increased after SP7 overexpression, and LRP5 inhibition decreased the number of mineralized nodules. SP7 overexpression prevented LRP5 inhibition and increased the number of mineralized nodules on Day 21. Furthermore, the results of qPCR and western blot indicated that the expression levels of LRP5, β-catenin, and osteogenic markers Runx2 and SP7 were significantly repressed in the LRP5 group (Figs. 5c and 5d). SP7 overexpression significantly rescued the decreased expression of osteogenic

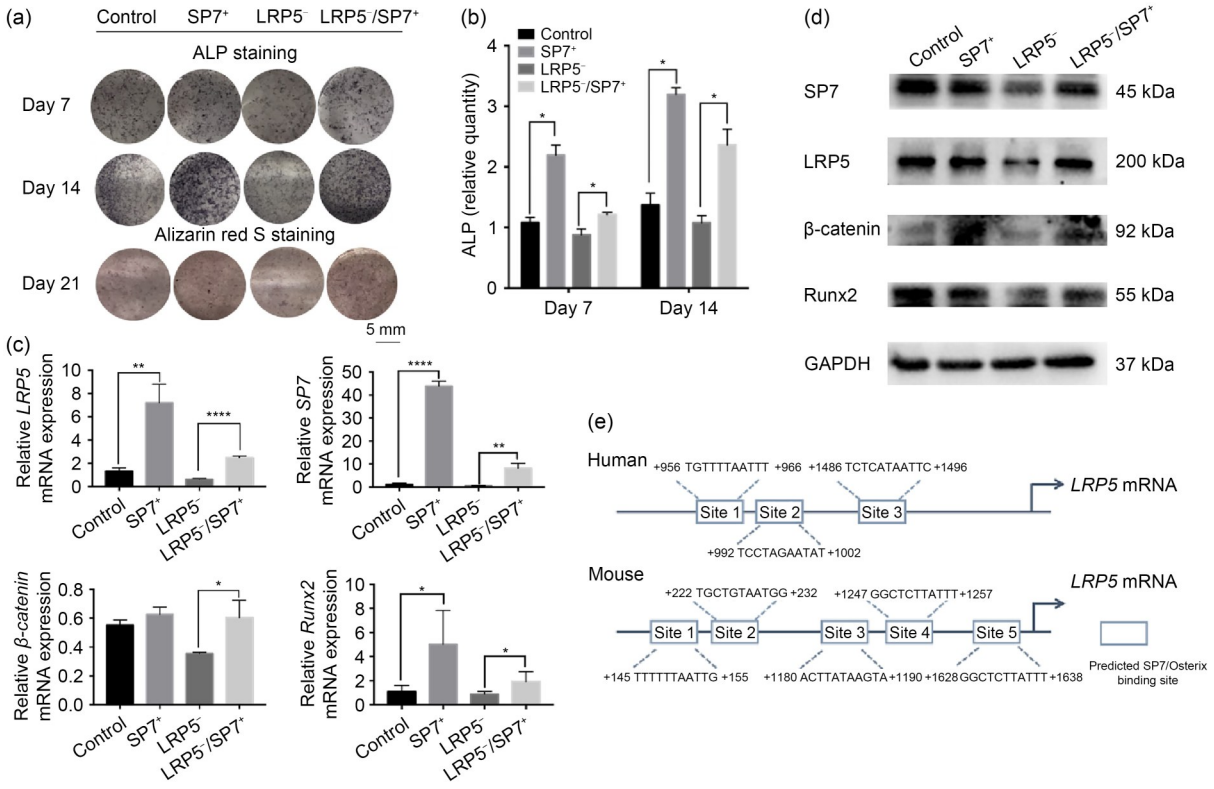

Fig. 5 Effect of SP7 on *LRP5* gene expression, thereby upregulating the osteogenic transcriptional network. (a) The alkaline phosphatase (ALP) staining was performed to evaluate the early osteogenic ability of mouse bone marrow mesenchymal stem cells (BMSCs) on osteogenic Day 7 and Day 14 after co-transfection of $LRP5^-$ and $SP7^+$. Alizarin red S staining was carried out to visualize the Ca nodules of mouse BMSCs on osteogenic Day 21 after the co-transfection of $LRP5^-$ and $SP7^+$. (b) The ALP activity of the $LRP5^-/SP7^+$ group was significantly increased compared to that of $LRP5^-$ group. (c) The quantitative real-time polymerase chain reaction (qPCR) analysis of relative messenger RNA (mRNA) expression of *SP7*, *LRP5*, *β-catenin*, and Runt-related transcription factor 2 (*Runx2*) on osteogenic Day 7 after co-transfection of $LRP5^-$ and $SP7^+$ in mouse BMSCs. (d) Western blot analysis showed the protein expression of SP7, LRP5, Runx2, and β-catenin on osteogenic Day 7 after the co-transfection of $LRP5^-$ and $SP7^+$ in mouse BMSCs. (e) Prediction of binding sites using the JASPER program. Data are expressed as mean±standard deviation (SD) (n=3). * P<0.05, ** P<0.01, **** P<0.0001. SP7: transcription factor osterix; LRP5: low-density lipoprotein receptor-related protein 5; GAPDH: glyceraldehyde 3-phosphate dehydrogenase.

genes caused by LRP5 interference. To explore the regulation between SP7 and LRP5, sequences were analyzed using the JASPER program (Khan et al., 2018). LRP5 regulatory elements share homology to known SP7-binding sites (Fig. 5e). The findings suggested that SP7 might be a direct transcriptional regulator that promoted *LRP5* gene expression, and *SP7* could be a promising therapeutic gene to ameliorate LRP5-dependent osteoporosis.

3.5 Role of SP7 viral therapy on defect healing in adult mice lacking LRP5 in vivo

In order to verify whether SP7 overexpression viral therapy can ameliorate osteogenesis in LRP5-dependent osteoporosis in vivo, a tibial defect model was constructed. The SP7-overexpressing virus was transfected into WT and cKO mouse defect sites (Xiang et al., 2017). Micro-CT analysis was performed to evaluate new bone formation in the defect areas of each group at four weeks after surgery (Figs. 6a and 6b). The BMD and BV/TV of the WT $SP7^+$ group were higher than those of the WT Blank and WT LVNC groups, but the differences were not statistically significant. The BMD and BV/TV of the cKO $SP7^+$ group were significantly higher than those of the cKO Blank and cKO LVNC groups. To investigate the rates of mineralized bone formation in the defect areas of each group, alizarin and calcein were administered for fluorochrome labeling 10 d and 3 d before sacrifice (Fig. 6c). The mineral apposition rate (MAR) of the WT $SP7^+$ group was higher than those of the WT Blank and WT LVNC groups, but the difference was not statistically significant. The MAR of the cKO $SP7^+$ group was significantly higher than that of the cKO Blank group, but not significantly different from that of the cKO LVNC group (Fig. 6d). These results indicated that SP7 therapy could improve tibial defect healing in mice lacking LRP5 in vivo, indicating the potential value of *SP7* as a therapeutic gene for osteoporosis.

4 Discussion

Emerging evidence points to SP7 as a vital transcription factor in the osteogenic differentiation of osteoblasts and bone healing. *SP7* gene delivery has been reported to effectively induce bone differentiation (Tu et al., 2007; Wang et al., 2013; Kim et al., 2021) and BMSC-associated osseointegration of implants (Xu et al., 2009). However, no studies have yet evaluated the role and underlying mechanisms of SP7 therapy in ameliorating osteogenesis for LRP5-dependent osteoporosis in vivo. Our study demonstrated that the viral delivery of SP7 could ameliorate compromised osteogenesis attributed to LRP5 deficiency by directly upregulating the suboptimal expression of LRP5. Moreover, we presented evidence that defect healing was impaired in cKO mice, and local administration of the SP7 overexpression virus markedly enhanced the formation of new bone during the bone defect repair process in adult mice lacking LRP5 (Fig. 7).

Consistent with previous results (Cui et al., 2011), abnormal bone tissues and impaired bone quality were found in cKO mice in the present study. We also established that bone defect healing was impaired due to LRP5 deficiency. A recent study reported similar activation of Wnt signaling within mesenchymal cells during bone defect healing in adult mouse skeletons (He et al., 2023). Thus, Wnt signaling is considered essential for both skeletal development and postnatal bone regeneration. The phenotype of *LRP5* cKO mice corroborated our in vitro observation that the loss of LRP5 in mature osteoblasts led to the low expression of osteogenic-related genes. Of note, the expression of SP7 was also reduced in *LRP5* cKO mice.

Considerable progress has been made regarding our understanding of functional links between LRP5 and SP7. Our recent study indicated that bidirectional regulation between SP7 and LRP5 is involved in circular RNA422 (circRNA422)-mediated early osseointegration of the implant (Yu et al., 2022). In this study, to investigate the potential role of SP7 therapy in ameliorating LRP5-dependent osteoporosis, we locally injected SP7 lentivirus into the tibia defect sites of WT and cKO mice. In vivo experiments revealed that the SP7 overexpression viral therapy promoted the formation of new bone during bone defect repair. The identification of the robust effects of SP7 overexpression virus in cKO suggests that LRP5-related diseases characterized by a relative or absolute decrease in bone formation might reap significant bone-building benefits from SP7 therapy. Therefore, SP7 overexpression viral delivery may ameliorate osteoporosis caused by the insufficient expression of LRP5, providing a novel therapeutic avenue for diseases characterized by a relative or absolute decrease in bone formation. We

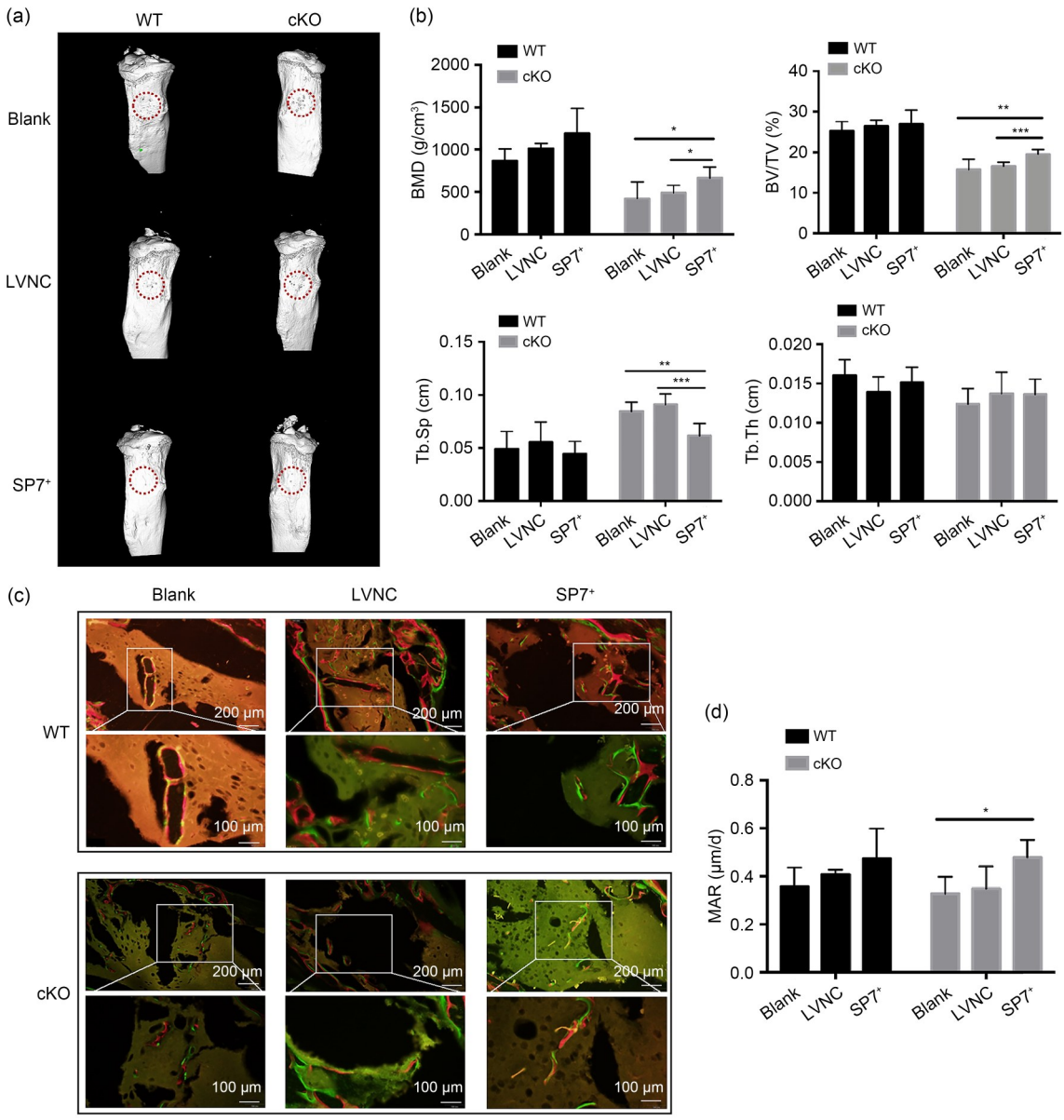

Fig. 6 Role of SP7 viral therapy on tibia defect healing in adult mice lacking LRP5 in vivo. (a) The representative images of micro-computed tomography (micro-CT) reconstruction from six groups were observed and recorded four weeks after surgery. (b) Quantitative micro-CT analyses of the area of tibial defects from six groups. (c) Images of fluorochrome labeling in the area of tibial defects from six groups. (d) Mineral apposition rate (MAR) of the conditional knockout (cKO) SP7$^+$ group was significantly higher than that of the cKO Blank group, but not significantly different from that of the cKO LVNC group. Data are expressed as mean±standard deviation (SD) (n=6). * P<0.05, ** P<0.01, *** P<0.001. SP7: transcription factor osterix; LRP5: low-density lipoprotein receptor-related protein 5; WT: wild-type; LVNC group: mice injected with 1 μL of LVNC into the prepared holes in the tibias; BMD: bone mineral density; BV/TV: bone volume to tissue volume; Tb.Th: trabecular thickness; Tb.Sp: trabecular separation.

further analyzed the sequences from mouse or human samples using the JASPER program (Khan et al., 2018) and predicted that the LRP5 regulatory element and SP7-binding site were homologous. However, it remains to be determined how the precise genomic binding sites of SP7 are specific to LRP5 and how SP7 binding ultimately relates to the regulation of LRP5 transcription.

Transcription factors are used for therapy either in protein form or as genetic materials encoded in suitable gene vectors (plasmid DNA and mRNA in viral vectors) (Kootstra and Verma, 2003; Ledo et al., 2020).

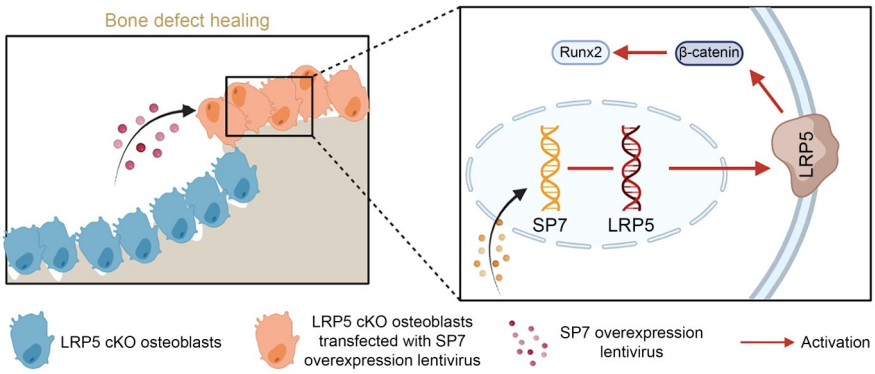

Fig. 7 Mechanisms of transcription factor osterix (SP7)-based therapy underlying bone defect healing in low-density lipoprotein receptor-related protein 5 (LRP5)-dependent osteoporosis mice.

In this study, the local delivery of SP7 was achieved by local administration of *SP7* mRNA overexpression virus in the tibia defect area. mRNA gene therapy has been reported as a promising alternative leading to a higher level of tissue regeneration (Wang et al., 2020; Wisitrasameewong et al., 2022). Compared to the delivery of DNA, recombinant proteins, and peptides, mRNA therapy is considered more efficient and suitable in non-dividing cells, since mRNA is directly translated inside the cytoplasm (Wisitrasameewong et al., 2022). However, the instability and immunogenicity of mRNA largely limit its application in vivo (Bleich et al., 2012; Schlake et al., 2019). In future studies, effective approaches to increase the stability and translatability of *SP7* mRNA and decrease the high immunogenicity of this type of therapy need to be explored. The introduction of modified nucleosides into in vitro transcribed mRNA has been proven to be effective in solving the above problems (Karikó et al., 2005). Furthermore, a systemic treatment approach remains to be explored to deliver *SP7* mRNA targeting whole-body bone tissue in LRP5-dependent osteoporosis mice. Recombinant adeno-associated virus 9 (rAAV9) has been reported to be highly effective for transducing osteoblasts in the bone (He et al., 2023). Thus, the systemic delivery of SP7 targeting osteoblasts might be achieved via rAAV9 or improved rAAV9 in future work.

In addition, the fat content in the bone marrow cavity of knockout mice was relatively increased and bone resorption was accelerated in cKO mice compared with their control littermates. Previous studies have reported that the upregulation of peroxisome proliferator-activated receptor gamma (PPARG) and the downregulation of Runx2 in osteoblasts induced the transdifferentiation of osteoblasts to adipocytes (Kim et al., 2016). Song LG et al. (2012) further confirmed that the loss of Wnt/β-catenin signaling caused the transdifferentiation of osteoblasts to adipocytes. Hence, the inactivation of LRP5 in Ocn^{+} osteoblasts may induce the transdifferentiation of osteoblasts into adipocytes, leading to augmented adiposity within the bone marrow. However, the mechanisms underlying increased marrow adiposity formation need to be explored in future studies.

5 Conclusions

In summary, we observed that SP7 enhanced the bone defect healing process by upregulating insufficient LRP5 expression, and the physical and functional interaction between LRP5 and SP7 was confirmed. SP7 could promote *LRP5* gene expression, thereby upregulating the osteogenic transcriptional network. Our results suggest that SP7-mediated LRP5 activation could serve as a foundation for the development of therapeutic strategies aimed at improving conditions related to osteoporosis and facilitating bone repair.

Data availability statement

The data supporting the findings of this study are available within the article and its supplementary materials. Should any raw data files be needed in another format, they are available from the corresponding author upon reasonable request.

Acknowledgments

This work was supported by the National Natural Science Foundation of China (No. 82101061) and the Science and Technology Department of Zhejiang Province (No. 2021C03113), China.

Author contributions

Ying WANG, Guoli YANG, Yue XI, and Qifeng JIANG performed the study concept; Wei DAI, Chaozhen CHEN, and Yang WANG provided acquisition, analysis, and interpretation of data; Kaichen LAI, Xiaoyan MIAO, and Zhiwei JIANG performed the development of methodology; Yue XI and Qifeng JIANG performed statistical analysis and writing. All authors have read and approved the final manuscript, and therefore, take responsibility for the integrity and security of the data.

Compliance with ethics guidelines

Zhiwei JIANG is a Young Scientist Committee Member for *Journal of Zhejiang University-SCIENCE B (Biomedicine & Biotechnology)* and was not involved in the editorial review or the decision to publish this article. Yue XI, Qifeng JIANG, Wei DAI, Chaozhen CHEN, Yang WANG, Xiaoyan MIAO, Kaichen LAI, Zhiwei JIANG, Guoli YANG, and Ying WANG declare that they have no conflict of interest.

All institutional and national guidelines for the care and use of laboratory animals were followed.

References

Baron R, Kneissel M, 2013. WNT signaling in bone homeostasis and disease: from human mutations to treatments. *Nat Med*, 19(2):179-192. https://doi.org/10.1038/nm.3074

Bleich NK, Kallai I, Lieberman JR, et al., 2012. Gene therapy approaches to regenerating bone. *Adv Drug Deliv Rev*, 64(12):1320-1330. https://doi.org/10.1016/j.addr.2012.03.007

Cai H, Zhang HM, He WT, et al., 2023. Iron accumulation and its impact on osteoporotic fractures in postmenopausal women. *J Zhejiang Univ-Sci B (Biomed & Biotechnol)*, 24(4):301-311. https://doi.org/10.1631/jzus.B2200519

Castrogiovanni P, Trovato FM, Szychlinska MA, et al., 2016. The importance of physical activity in osteoporosis. From the molecular pathways to the clinical evidence. *Histol Histopathol*, 31(11):1183-1194. https://doi.org/10.14670/Hh-11-793

Cauley JA, Giangregorio L, 2020. Physical activity and skeletal health in adults. *Lancet Diabetes Endocrinol*, 8(2): 150-162. https://doi.org/10.1016/S2213-8587(19)30351-1

Cui YJ, Niziolek PJ, MacDonald BT, et al., 2011. Lrp5 functions in bone to regulate bone mass. *Nat Med*, 17(6):684-691. https://doi.org/10.1038/nm.2388

Fukuda M, Yoshizawa T, Karim MF, et al., 2018. SIRT7 has a critical role in bone formation by regulating lysine acylation of SP7/osterix. *Nat Commun*, 9:2833. https://doi.org/10.1038/s41467-018-05187-4

Gong YQ, Slee RB, Fukai N, et al., 2001. LDL receptor-related protein 5 (LRP5) affects bone accrual and eye development. *Cell*, 107(4):513-523. https://doi.org/10.1016/s0092-8674(01)00571-2

Hafner M, Zimmermann K, Pottgiesser J, et al., 1995. A purine-rich sequence in the human BM-40 gene promoter region is a prerequisite for maximum transcription. *Matrix Biol*, 14(9):733-741. https://doi.org/10.1016/S0945-053x(05)80016-2

He GP, Nie JJ, Liu X, et al., 2023. Zinc oxide nanoparticles inhibit osteosarcoma metastasis by downregulating β-catenin via HIF-1α/BNIP3/LC3B-mediated mitophagy pathway. *Bioact Mater*, 19:690-702. https://doi.org/10.1016/j.bioactmat.2022.05.006

Hill TP, Später D, Taketo MM, et al., 2005. Canonical Wnt/β-catenin signaling prevents osteoblasts from differentiating into chondrocytes. *Dev Cell*, 8(5):727-738. https://doi.org/10.1016/j.devcel.2005.02.013

Hofbauer LC, Maisch B, Schaefer JR, 2002. High bone density due to a mutation in LDL-receptor-related protein 5. *N Engl J Med*, 347(12):943-944. https://doi.org/10.1056/NEJM200209193471216

Hoshikawa S, Shimizu K, Watahiki A, et al., 2020. Phosphorylation-dependent osterix degradation negatively regulates osteoblast differentiation. *FASEB J*, 34(11):14930-14945. https://doi.org/10.1096/fj.202001340R

Jiang ZW, Wang HM, Yu K, et al., 2017. Light-controlled BMSC sheet-implant complexes with improved osteogenesis via an LRP5/β-catenin/Runx2 regulatory loop. *ACS Appl Mater Interfaces*, 9(40):34674-34686. https://doi.org/10.1021/acsami.7b10184

Jiang ZW, Yu K, Feng YT, et al., 2020. An effective light activated TiO_2 nanodot platform for gene delivery within cell sheets to enhance osseointegration. *Chem Eng J*, 402: 126170. https://doi.org/10.1016/j.cej.2020.126170

Karikó K, Buckstein M, Ni HP, et al., 2005. Suppression of RNA recognition by Toll-like receptors: the impact of nucleoside modification and the evolutionary origin of RNA. *Immunity*, 23(2):165-175. https://doi.org/10.1016/j.immuni.2005.06.008

Katchkovsky S, Chatterjee B, Abramovitch-Dahan CV, et al., 2022. Competitive blocking of LRP4-sclerostin binding interface strongly promotes bone anabolic functions. *Cell Mol Life Sci*, 79(2):113. https://doi.org/10.1007/s00018-022-04127-2

Khan A, Fornes O, Stigliani A, et al., 2018. JASPAR 2018: update of the open-access database of transcription factor binding profiles and its web framework. *Nucleic Acids Res*, 46(D1):D1284. https://doi.org/10.1093/nar/gkx1188

Kim HJ, Lee S, Park JM, et al., 2021. Development of a three-layer consecutive gene delivery system for enhanced bone regeneration. *Biomaterials*, 277:121104. https://doi.org/10.1016/j.biomaterials.2021.121104

Kim JH, Seong S, Kim K, et al., 2016. Downregulation of Runx2 by 1,25-dihydroxyvitamin D_3 induces the transdifferentiation of osteoblasts to adipocytes. *Int J Mol Sci*, 17(5):770. https://doi.org/10.3390/ijms17050770

Knight MN, Karuppaiah K, Lowe M, et al., 2018. R-spondin-2 is a Wnt agonist that regulates osteoblast activity and bone mass. *Bone Res*, 6:24. https://doi.org/10.1038/s41413-018-0026-7

Kootstra NA, Verma IM, 2003. Gene therapy with viral vectors.

Annu Rev Pharmacol Toxicol, 43:413-439. https://doi.org/10.1146/annurev.pharmtox.43.100901.140257

Lambert SA, Jolma A, Campitelli LF, et al., 2018. The human transcription factors. *Cell*, 175(2):598-599. https://doi.org/10.1016/j.cell.2018.09.045

Ledo AM, Senra A, Rilo-Alvarez H, et al., 2020. mRNA-activated matrices encoding transcription factors as primers of cell differentiation in tissue engineering. *Biomaterials*, 247: 120016. https://doi.org/10.1016/j.biomaterials.2020.120016

Lee TI, Young RA, 2013. Transcriptional regulation and its misregulation in disease. *Cell*, 152(6):1237-1251. https://doi.org/10.1016/j.cell.2013.02.014

Leucht P, Lee S, Yim N, 2019. Wnt signaling and bone regeneration: can't have one without the other. *Biomaterials*, 196:46-50. https://doi.org/10.1016/j.biomaterials.2018.03.029

Lim WH, Liu B, Mah SJ, et al., 2015. Alveolar bone turnover and periodontal ligament width are controlled by Wnt. *J Periodontol*, 86(2):319-326. https://doi.org/10.1902/jop.2014.140286

Little RD, Folz C, Manning SP, et al., 2002. A mutation in the LDL receptor-related protein 5 gene results in the autosomal dominant high-bone-mass trait. *Am J Hum Genet*, 70(1): 11-19. https://doi.org/10.1086/338450

Lui JC, Raimann A, Hojo H, et al., 2022. A neomorphic variant in SP7 alters sequence specificity and causes a high-turnover bone disorder. *Nat Commun*, 13:700. https://doi.org/10.1038/s41467-022-28318-4

Mead TJ, 2020. Alizarin red and Alcian blue preparations to visualize the skeleton. *Methods Mol Biol*, 2043:207-212. https://doi.org/10.1007/978-1-4939-9698-8_17

Muñoz-Garach A, García-Fontana B, Muñoz-Torres M, 2020. Nutrients and dietary patterns related to osteoporosis. *Nutrients*, 12(7):1986. https://doi.org/10.3390/nu12071986

Nakashima K, Zhou X, Kunkel G, et al., 2002. The novel zinc finger-containing transcription factor osterix is required for osteoblast differentiation and bone formation. *Cell*, 108(1):17-29. https://doi.org/10.1016/s0092-8674(01)00622-5

Rigueur D, Lyons KM, 2014. Whole-mount skeletal staining. *Methods Mol Biol*, 1130:113-121. https://doi.org/10.1007/978-1-62703-989-5_9

Rilo-Alvarez H, Ledo AM, Vidal A, et al., 2021. Delivery of transcription factors as modulators of cell differentiation. *Drug Deliv Transl Res*, 11(2):426-444. https://doi.org/10.1007/s13346-021-00931-8

Schlake T, Thess A, Thran M, et al., 2019. mRNA as novel technology for passive immunotherapy. *Cell Mol Life Sci*, 76(2):301-328. https://doi.org/10.1007/s00018-018-2935-4

Song KH, Nam YJ, Luo X, et al., 2012. Heart repair by reprogramming non-myocytes with cardiac transcription factors. *Nature*, 485(7400):599-604. https://doi.org/10.1038/nature11139

Song LG, Liu ML, Ono N, et al., 2012. Loss of Wnt/β-catenin signaling causes cell fate shift of preosteoblasts from osteoblasts to adipocytes. *J Bone Miner Res*, 27(11):2344-2358. https://doi.org/10.1002/jbmr.1694

Tu QS, Valverde P, Li S, et al., 2007. Osterix overexpression in mesenchymal stem cells stimulates healing of critical-sized defects in murine calvarial bone. *Tissue Eng*, 13(10): 2431-2440. https://doi.org/10.1089/ten.2006.0406

Wang B, Huang SY, Pan LN, et al., 2013. Enhancement of bone formation by genetically engineered human umbilical cord-derived mesenchymal stem cells expressing osterix. *Oral Surg Oral Med Oral Pathol Oral Radiol*, 116(4): e221-e229. https://doi.org/10.1016/j.oooo.2011.12.024

Wang JS, Kamath T, Mazur CM, et al., 2021. Control of osteocyte dendrite formation by Sp7 and its target gene osteocrin. *Nat Commun*, 12:6271. https://doi.org/10.1038/s41467-021-26571-7

Wang PP, Logeart-Avramoglou D, Petite H, et al., 2020. Co-delivery of NS1 and BMP2 mRNAs to murine pluripotent stem cells leads to enhanced BMP-2 expression and osteogenic differentiation. *Acta Biomater*, 108:337-346. https://doi.org/10.1016/j.actbio.2020.03.045

Wisitrasameewong W, Champaiboon C, Surisaeng T, et al., 2022. The impact of mRNA technology in regenerative therapy: lessons for oral tissue regeneration. *J Dent Res*, 101(9):1015-1024.

Witcher PC, Miner SE, Horan DJ, et al., 2018. Sclerostin neutralization unleashes the osteoanabolic effects of Dkk1 inhibition. *JCI Insight*, 3(11):e98673. https://doi.org/10.1172/jci.insight.98673

Xiang L, Ma L, Wei N, et al., 2017. Effect of lentiviral vector overexpression α-calcitonin gene-related peptide on titanium implant osseointegration in α-CGRP-deficient mice. *Bone*, 94:135-140. https://doi.org/10.1016/j.bone.2015.08.009

Xu B, Zhang J, Brewer E, et al., 2009. Osterix enhances BMSC-associated osseointegration of implants. *J Dent Res*, 88(11):1003-1007. https://doi.org/10.1177/0022034509346928

Xu JK, Hu PJ, Zhang XT, et al., 2022. Magnesium implantation or supplementation ameliorates bone disorder in CFTR-mutant mice through an ATF4-dependent Wnt/β-catenin signaling. *Bioact Mater*, 8:95-108. https://doi.org/10.1016/j.bioactmat.2021.06.034

Yu K, Jiang ZW, Miao XY, et al., 2022. circRNA422 enhanced osteogenic differentiation of bone marrow mesenchymal stem cells during early osseointegration through the SP7/LRP5 axis. *Mol Ther*, 30(10):3226-3240. https://doi.org/10.1016/j.ymthe.2022.05.020

Zhong ZD, Zylstra-Diegel CR, Schumacher CA, et al., 2012. Wntless functions in mature osteoblasts to regulate bone mass. *Proc Natl Acad Sci USA*, 109(33):E2197-E2204. https://doi.org/10.1073/pnas.1120407109

Supplementary information

Fig. S1; Tables S1 and S2